Journal of Solid State Chemistry **163,** 137–143 (2002)
doi:10.1006/jssc.2001.9383, available online at http://www.idealibrary.com on IDEAL®

In Situ Oxidation of $Nb_{22}O_{54}$ in a Gas Reaction Cell High-Resolution Transmission Electron Microscope

M. J. Sayagués*,[1] and J. L. Hutchison†

*Instituto de Ciencia de Materiales de Sevilla, Avda. Américo Vespucio s/n, Isla de la Cartuja, 41092 Sevilla, Spain; and †Department of Materials, University of Oxford, Parks Road, Oxford OX1 3PH U.K.

Received March 27, 2001; in revised form August 21, 2001; accepted August 30, 2001; published online November 27, 2001

A nonstoichiometric block structure oxide, $Nb_{22}O_{54}$ ($NbO_{2.455}$), with monoclinic symmetry was characterized following *in situ* oxidation in a controlled environment, high-resolution electron microscope. This instrument is based on a JEOL 4000EX electron microscope equipped with a gas reaction cell. The oxidation reaction was carried out by introducing ca. 20 mb of oxygen gas to the specimen region and heating the specimen by means of a focussed electron beam. The resulting structures obtained after the oxidation reaction were not totally homogeneous. (1) Mainly microdomains of $Nb_{10}O_{25}$ were found, which consists of [3 × 3] blocks of octahedra linked through tetrahedrally coordinated sites—such a structure is isostructural with PNb_9O_{25}. $Nb_{10}O_{25}$ seems to be a metastable phase in the Nb–O system, and was found here for the first time as extended domains. (2) A highly disordered structure was observed in some areas of the crystal after oxidation, with a corresponding electron diffraction pattern similar to an "X" phase interpreted as two-dimensionally disordered H-Nb_2O_5. Very clear lamellar defects were also found after oxidation.

1. INTRODUCTION

High-resolution electron microscopy (HREM) studies (1–3) have demonstrated that the lattice imaging technique can provide atomic scale information in complex oxides. Today it is also possible to track by direct observation the atomic movements which occur in the course of a solid-state reaction by using a controlled environment transmission electron microscope (CETEM). It is a combination of a gas reaction cell (GRC, also designated as an environmental cell) and a high-resolution transmission electron microscope (4, 5). This technique represents a relatively recent development which allows real-time observation of structural changes at the atomic level (6–14).

[1] To whom correspondence should be addressed. E-mail: sayagues@cica.es.

$Nb_{22}O_{54}$ has a block structure (15, 16) with monoclinic symmetry (Fig. 1). It is formed by [4 × 3] blocks of corner-linked NbO_6 octahedra (connected at the same height by sharing edges) alternating with [3 × 3] blocks (connected by tetrahedral sites occupied by Nb^{5+}). It can also be considered as a 1:1 intergrowth of $Nb_{12}O_{29}$ and a hypothetical $Nb_{10}O_{25}$ structure, which is isostructural to PNb_9O_{25} (17).

The initial idea was to study the structural changes from $Nb_{12}O_{29}$ ($NbO_{2.4167}$) to $Nb_{22}O_{54}$ ($NbO_{2.4545}$) to $Nb_{10}O_{25}$ ($NbO_{2.5000}$) and to carry out the *in situ* oxidation process in one experiment. However, due to experimental inconveniences we have divided the experiment in two steps. The first one corresponds to the oxidation of $Nb_{12}O_{29}$ to $Nb_{22}O_{54}$ and the obtained results were published in a previous paper (13); it was not possible to proceed further in the *in situ* oxidation reaction due to the contamination of the specimen and its support film produced by the gas introduced into the GRC. The current work is focused on the latter step of the oxidation reaction, going from $Nb_{22}O_{54}$ to $Nb_{10}O_{25}$. A $Nb_{22}O_{54}$ sample has been oxidized *in situ* in the gas reaction cell microscope and the analysis of the results of such an experiment are presented and discussed.

2. EXPERIMENTAL

Samples for HREM were prepared by dispersing a suspension of the powder in acetone onto a holey carbon film supported by a copper grid. Finder grids were used to allow us to locate and analyze the same crystallite with different microscopes. The oxidation reaction was done using a JEOL 4000EX gas reaction cell microscope (4) (side-entry configuration); the microscope operates at 400 kV with a LaB_6 filament. The point resolution is about 0.26 nm in a vacuum; with the crystal under a gaseous environment the point resolution is reduced to 0.3 nm.

Although the resolution of the GRC microscope is sufficient to reveal the structural changes, it fails in same cases due to the contamination problems after the gas reaction.

0022-4596/02 $35.00

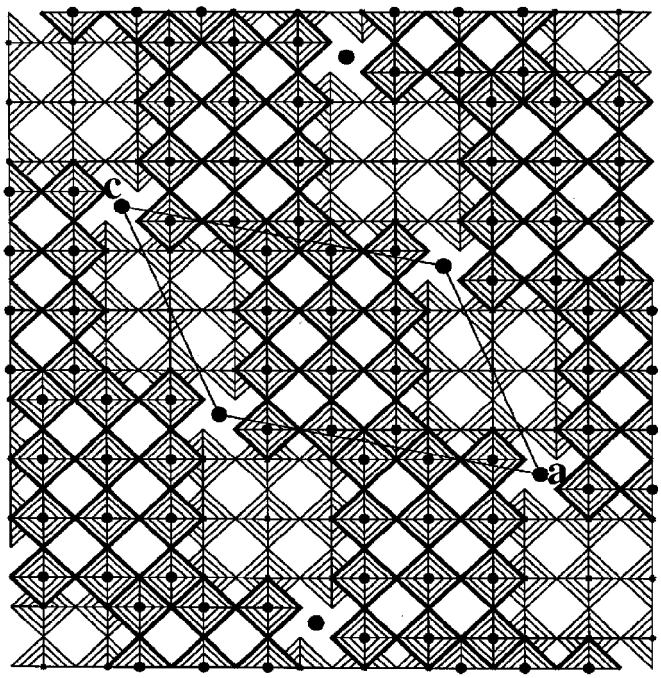

FIG. 1. Structural model in the **ac** projection of $Nb_{22}O_{54}$. The black dots represent Nb^{5+} cations located in tetrahedral coordination.

Therefore, some of the crystallites were reinvestigated after the *in situ* reaction in another JEOL 4000EX microscope ($V_{acc} = 400$ kV, LaB_6 filament) which is equipped with a top-entry goniometer that provides a point resolution of 0.16 nm.

In the following experiments, suitable crystals were located with the cell under a vacuum and orientated in the [010] zone axis. Oxygen gas was then introduced into the specimen area and the electron beam was used to heat the crystal locally (by changing the condenser aperture or even removing it in order to increase the beam intensity). The images were recorded at magnification 300,000× and 400,000× at close to Scherzer focus. The image contrast in correctly oriented thin crystal regions corresponds to the projected crystal potential: the positions of the projected columns of heavy atoms appear dark and the tunnels appear bright (9).

3. RESULTS AND DISCUSSION

Figures 2a and 2b show a $Nb_{22}O_{54}$ GRC micrograph in a vacuum and the corresponding selected area electron diffraction (SAED) pattern, respectively. The streaking in the SAED pattern arises as a result of extra rows of 4×3 octahedra (Wadsley defects), indicated with arrows in Fig. 2a. The image contrast of $Nb_{22}O_{54}$ is formed by a sequence of $[3 \times 2]$ and $[2 \times 2]$ arrays of white dots (coming from the channels in the corresponding block, according to the structure arrangement of one row of $[4 \times 3]$ blocks alternating along the **a** axis with another of $[3 \times 3]$ blocks). The black contrast between $[2 \times 2]$ dots along the [001] direction corresponds to Nb atoms in tetrahedrally coordinated sites, which are located at the origin of the unit cell (marked with white lines). The $Nb_{22}O_{54}$ structural model is superimposed in an area (on the left) of the micrograph.

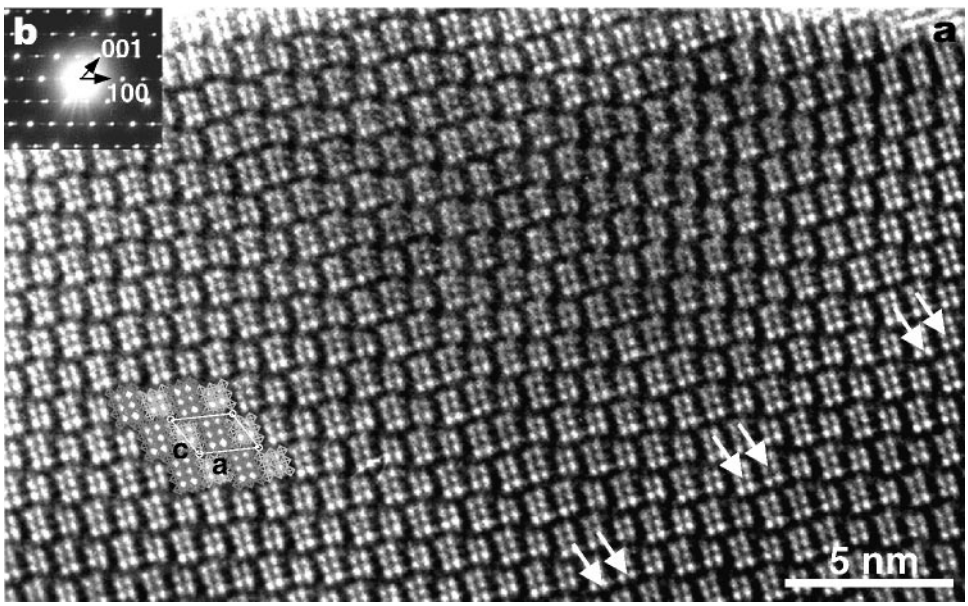

FIG. 2. (a) GRC micrograph of a $Nb_{22}O_{54}$ crystal under vacuum along [010]. A structural model is superimposed at the right side. (b) Corresponding SAED pattern.

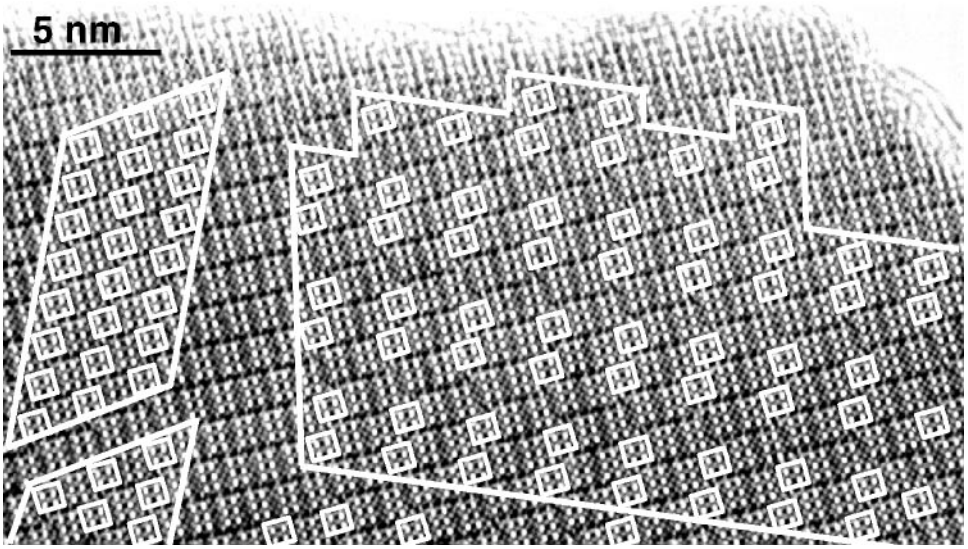

FIG. 3. HRTEM image of a $Nb_{22}O_{54}$ crystal under vacuum along [010] showing well-ordered intergrowths between $[4 \times 3]$ and $[3 \times 3]$ blocks.

We also found in vacuum a few crystals showing intergrowths, which were further analyzed in the HRTEM microscope. Figure 3 shows a HRTEM image where small domains of ordered intergrowths of $[4 \times 3]$ and $[3 \times 3]$ blocks can be clearly seen. The last one is marked with white squares indicating the periodicity of the formed intergrowths. On the left side, the periodicity between the two kinds of blocks corresponds to the $Nb_{22}O_{54}$ structure; however, the one on the right side corresponds to a much larger unit cell and different formula, intermediate between $Nb_{22}O_{54}$ and $Nb_{12}O_{29}$.

When the same crystal shown in Fig. 2a was treated with an oxygen atmosphere (15 mbar) in the GRC, alternating slabs of $Nb_{22}O_{54}$ and a new structure corresponding to $Nb_{10}O_{25}$ along [001] seems to be formed (Fig. 4) although the contrast of the new structure was not very clear due to the contamination problems. Another oxidized crystal was imaged (Fig. 5a) in the HRTEM and various $Nb_{10}O_{25}$

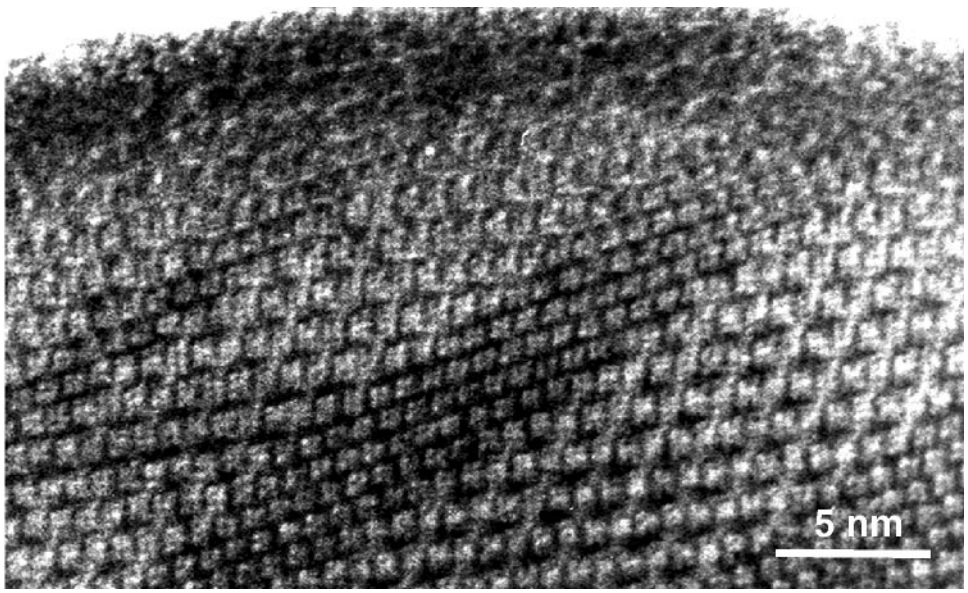

FIG. 4. (a) GRC micrograph of the same crystal shown in Fig. 2a after the oxidation process.

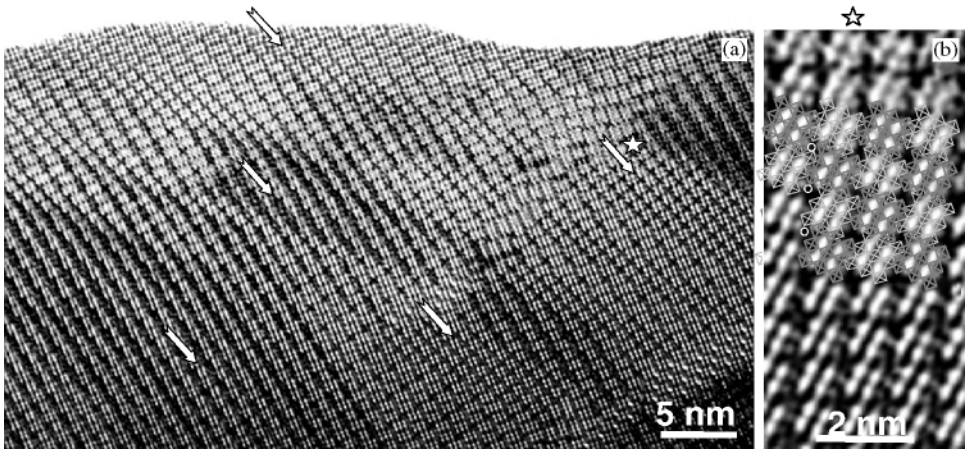

FIG. 5. (a) HRTEM micrograph of a $Nb_{22}O_{54}$ crystal after oxidation in the GRC. The $Nb_{10}O_{25}$ microdomains are marked with arrows. (b) Enlarged image of the area marked with a star in (a); the $Nb_{10}O_{25}$ structural model is superimposed.

domains are clearly observed (marked areas). The $[2 \times 2]$ white dots (from the $[3 \times 3]$ blocks of octahedra) are clearly visible and Nb^{5+} in the tetrahedral sites produced a black "X" array contrast in the image. The area marked with an asterisk has been enlarged and can be seen in Fig. 5b; a $Nb_{10}O_{25}$ structural model with tetragonal symmetry is superimposed. Regions where the contrast is very dark correspond to structures that are overlapping along the beam direction, as described previously by Hutchison (18).

It is worth noting that this $Nb_{10}O_{25}$ structure, a polymorph of Nb_2O_5 proposed by Roth *et al.* (17), has been observed here in the Nb–O binary system as a microdomain for the first time after the *in situ* oxidation reaction.

A very peculiar SAED pattern interpreted as a long-period modulation of the fundamental tetragonal unit comprising NbO_6 octahedra was found in some $Nb_{22}O_{54}$ crystals after oxidation and can be seen in Fig. 6a. This is very similar to a SAED pattern described by Kikuchi *et al.* (19) as a part of a mixture (named "X" phase), when a H-Nb_2O_5 sample was shocked perpendicularly to the **b** axis above 40 GPa. The GRC image corresponding to that peculiar SAED pattern is presented in Fig. 6b and shows a highly disordered structure. Two different areas marked in this micrograph (left and right) were enlarged and are shown in Figs. 7a and 7b, respectively. Coherent intergrowth of different block sizes ($[6 \times 3]$, $[5 \times 3]$, $[4 \times 3]$, $[4 \times 4]$, and $[3 \times 3]$)

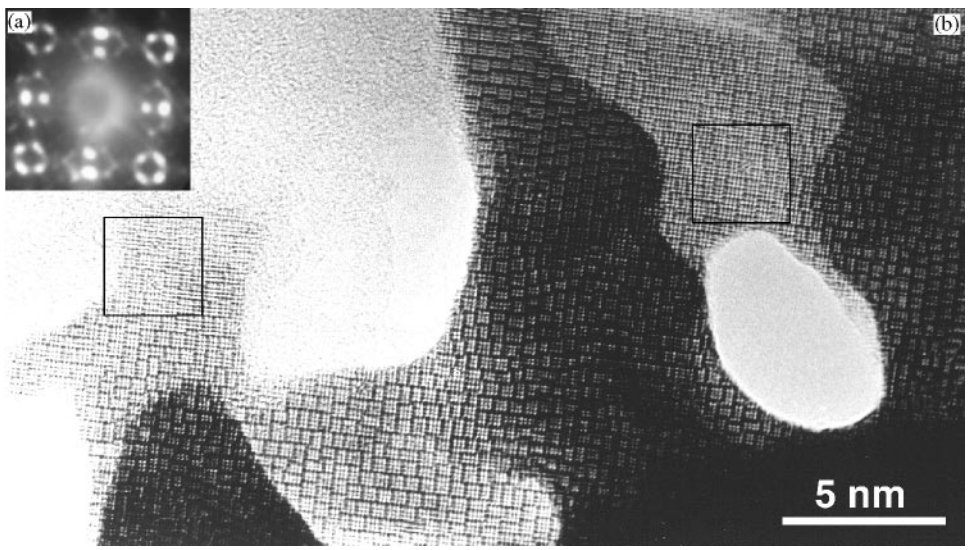

FIG. 6. (a) GRC micrograph of a $Nb_{22}O_{54}$ crystal after oxidation and (b) the corresponding SAED pattern. The two square areas marked in the image have been enlarged and can be seen in Fig. 7.

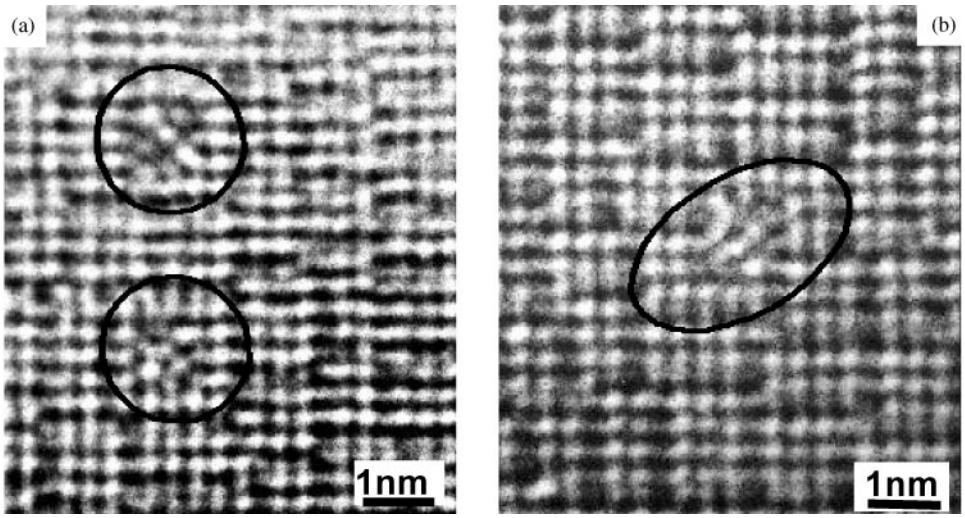

FIG. 7. Enlarged areas of the image presented in Fig. 6. Special contrast was found in the round marked areas.

can be clearly seen. In Fig. 7a, two large blocks (marked with circles) of $[6 \times 6]$ octahedra contain contrast, which suggests pairs of pentagonal columns (PCs) as found in tetragonal tungsten bronze structures (20). If correct, this is the first observation of PC structures within a block structure. Also, an unusual contrast feature (round marked area in Fig. 7b) that can be interpreted as a junction of two blocks giving place to a very bright anomalous contrast in the middle of the two blocks was found. It is clear that this "crystal" is in a highly disordered state, corresponding to a stage in the reaction when many atoms are highly mobile.

Some other crystals (found in the same sample) showing a composition between $Nb_{22}O_{54}$ and $Nb_{12}O_{29}$ were oxidized in the GRC microscope and then imaged in the HRTEM. Figure 8 shows the earliest stage of the oxidation reaction in one of these crystals, where only some lamellar defects can be seen (elliptic marked areas). Figure 9a presents another HR micrograph after oxidation where very clear lamellar defects between different kinds of blocks can be observed. Ordered rows of "rectangular tunnels" are formed, parallel to the original rows of tetrahedral sites (arrowed). As in a previous work (13) on oxidation of $Nb_{12}O_{29}$, these tunnels will provide a fast diffusion path into the reacting crystal. Following the image contrast in Fig. 9a, a structural model was built (Fig. 9b) to interpret the cation atomic distribution after the reaction under oxygen.

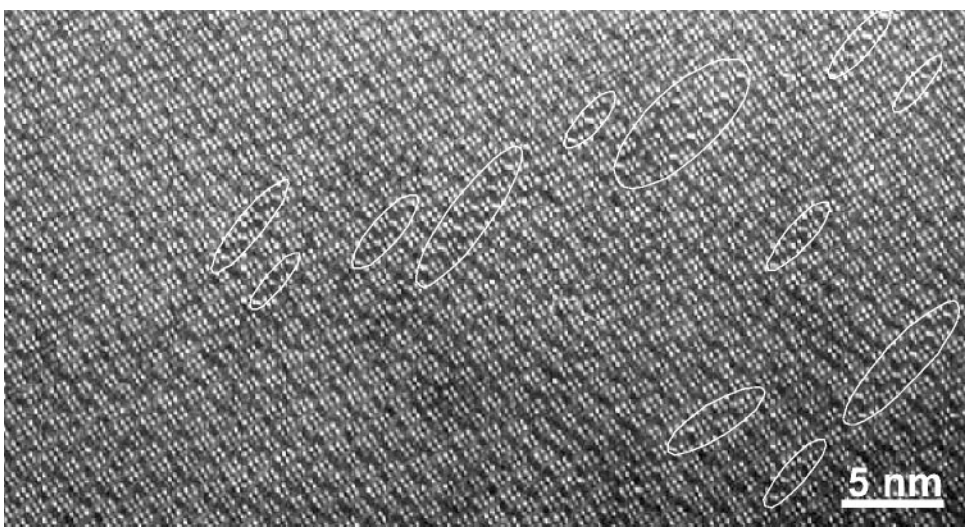

FIG. 8. HRTEM image after oxidation of a crystal with an intermediate formula between $Nb_{22}O_{54}$ and $Nb_{12}O_{29}$. It shows some lamellar defects as a first step of the reaction.

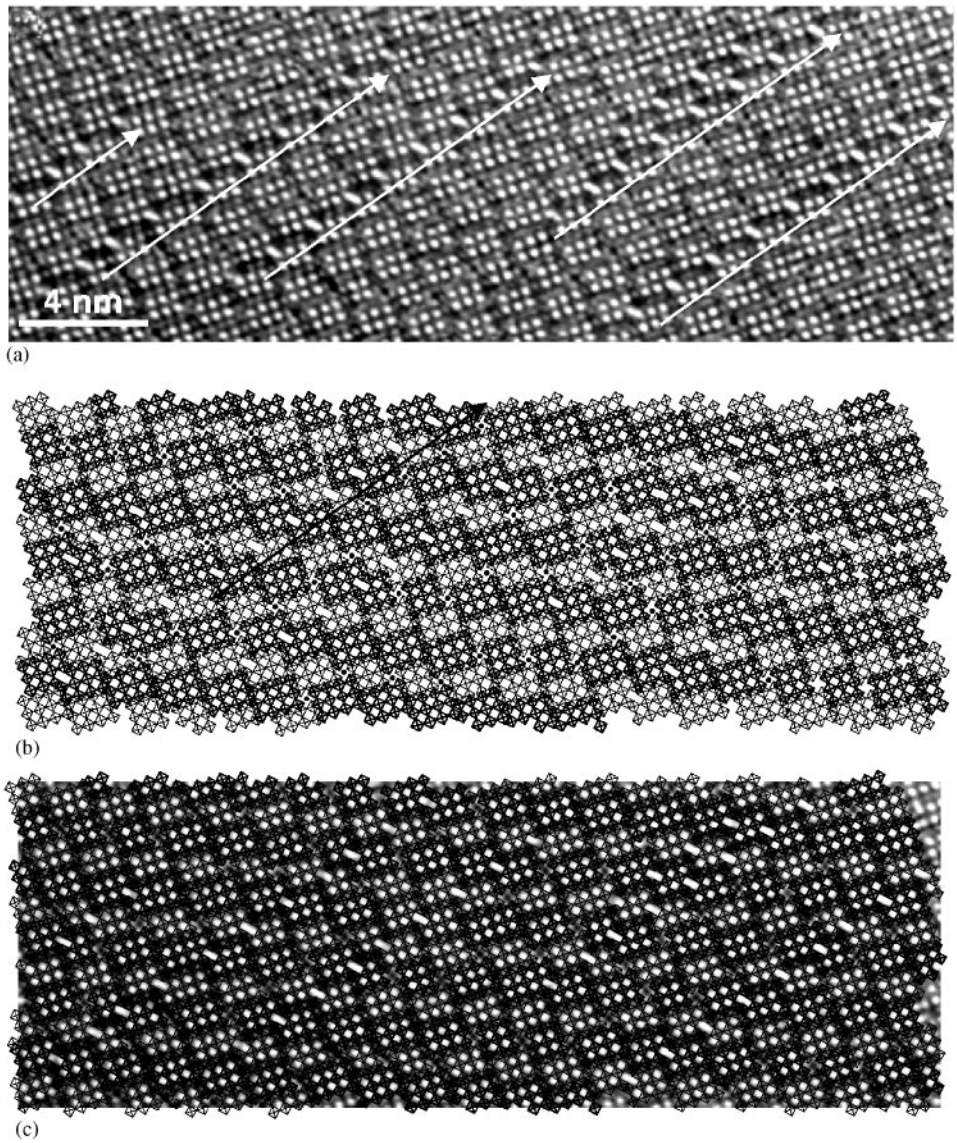

FIG. 9. (a) HRTEM image of a crystal (with an intermediate formula between $Nb_{22}O_{54}$ and $Nb_{12}O_{29}$) after oxidation. A very clear contrast of the changes after the reaction can be seen. (b) Structural model proposed for the above image contrast. (c) Matching of the image in (a) with the proposed structural model in (b).

The excellent matching between both the image and the structural model is shown in Fig. 9c. The creation of these rows of defects generates locally 3×3 blocks (i.e., $Nb_{10}O_{25}$), as well as 5×3 blocks linked by edge-sharing octahedra to the 4×3 blocks in the original structure.

4. CONCLUSIONS

The *in situ* oxidation of $Nb_{22}O_{54}$ crystals in the GRC microscope has led to $Nb_{10}O_{25}$ microdomains with tetragonal symmetry. This structure has been found for the first time in the binary Nb–O system.

Only when the crystals had an intermediate formula between $Nb_{22}O_{54}$ and $Nb_{12}O_{29}$ (found in the same sample) the *in situ* oxidation gave place to lamellar defects as an intermediate step in the oxidation process.

A very peculiar contrast interpreted as a pair of pentagonal columns as found in tetragonal tungsten bronzes was also observed after oxidation of $Nb_{22}O_{54}$ crystals.

Taking into account the previously published result (13), where the $Nb_{12}O_{29}$ was oxidized to $Nb_{22}O_{54}$, and the current paper dealing with the $Nb_{22}O_{54}$ to $Nb_{10}O_{25}$ oxidation, we can summarize that the structural changes are occurring gradually from one structure to the next (the three

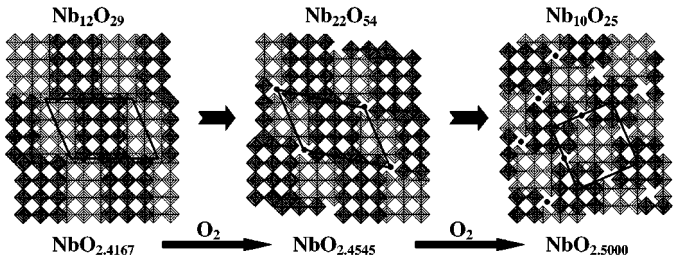

FIG. 10. Schematic representation of the following structural transformation represented on the **ac** projection: $Nb_{12}O_{29} \rightarrow Nb_{22}O_{54} \rightarrow Nb_{10}O_{25}$ after the *in situ* oxidation reaction in the GRC microscope. The lighter and darker squares represent NbO_6 octahedra that are centered on two different levels perpendicular to the **b** axis. The unit cells (**ac**) are outlined. The black dots represent Nb^{5+} cations located in tetrahedral coordination.

different structures are represented in Fig. 10). First, the oxygen produces lamellar defects providing an oxygen diffusion path for further oxidation. The heavy atoms are then shifted giving way to Nb^{5+} in tetrahedral coordination.

However, it has been also found that the oxidation reaction in these kinds of block structures leads to slightly different results and reacts at quite different rates depending on the defects in the original structure as well as on the thickness of the crystal.

ACKNOWLEDGMENTS

We thank NATO (Project CGR 97301118) for financial support and the head of the Oxford Materials Department for provision of laboratory facilities.

REFERENCES

1. S. Iijima and J. G. Allpress, *Acta Crystallogr. A* **30,** 22 (1974).
2. J. M. Browne, J. L. Hutchison, and J. S. Anderson, *Proc. 7th Symp. Reactivity Solids* 116 (1972).
3. F. Krumeich, *J. Solid State Chem.* **119,** 420 (1995).
4. R. C. Doole, G. M. Parkinson, and J. M. Stead, *Inst. Phys. Conf. Ser.* **118,** 157 (1991).
5. R. C. Doole, G. M. Parkinson, J. L. Hutchison, M. J. Goringe, and P. J. F. Harris, *JEOL News* **30E,** 30 (1992).
6. M. Goringe, A. Rawcliffe, A. Burden, J. L. Hutchison, and R. Doole, *Faraday Discuss. Chem. Soc.* **105,** 85 (1996).
7. M. J. Sayagués and J. L. Hutchison, *J. Solid State Chem.* **124,** 116 (1996).
8. E. D. Boyes and P. L. Gai, *Ultramicroscopy* **67,** 219 (1997).
9. P. L. Gai, *Acta Crystallogr. B* **53,** 346 (1997).
10. M. J. Sayagués and J. L. Hutchison, *in* "Electron Microscopy," Proceedings of the 14th ICEM, (C. Benavides and J. Yacamán, Eds.), III, Vol. 497. Institute of Physics Publishing, Bristol/Philadelphia, 1998.
11. A. Burden and J. L. Hutchison, *Carbon* **36,** 1167 (1998).
12. M. J. Sayagués, J. L. Hutchison, and F. Krumeich, *J. Solid State Chem.* **143,** 33 (1999).
13. M. J. Sayagués and J. L. Hutchison, *J. Solid State Chem.* **146,** 202 (1999).
14. F. Krumeich, J. L. Hutchison, and M. J. Sayagués, *Z. anorg. allg. Chem.* **625,** 755 (1999).
15. R. Norin, M. Carlsson, and B. Elgquist, *Acta Chem. Scand.* **20,** 2892 (1966).
16. S. Horiuchi and S. Kimura, *Jpn. J. Appl. Phys.* **21,** L97 (1982).
17. R. S. Roth, A. D. Wadsley, and S. Andersson, *Acta Crystallogr.* **18,** 643 (1965).
18. J. L. Hutchison, *in* "Proc. 6th European Congress on Electron Microscopy, Jerusalem" (D. G. Brandon, Ed.), Vol. 1, p. 147. 1976.
19. M. Kikuchi, K. Kusaba, E. Bannai, K. Fukuoka, Y. Syono, and K. Kiroga, *Jpn J. Appl. Phys.* **24,** 1600 (1985).
20. B. G. Hyde and M. O'Keeffe, *Acta Crystallogr. A* **29,** 243 (1973).